Hindawi
Journal of Spectroscopy
Volume 2021, Article ID 9968797, 8 pages
https://doi.org/10.1155/2021/9968797

Research Article

Experimental and Density Functional Theory Characteristics of Ibrutinib, a Bruton's Kinase Inhibitor Approved for Leukemia Treatment

Ali I. Ismail

Department of Chemistry, Rabigh College of Science and Arts, King Abdulaziz University, Jeddah, Saudi Arabia

Correspondence should be addressed to Ali I. Ismail; aeyesmaeel@kau.edu.sa

Received 21 March 2021; Revised 1 May 2021; Accepted 8 May 2021; Published 15 May 2021

Academic Editor: Vincenza Crupi

Ibrutinib, a Bruton's tyrosine kinase that plays an essential role in the B-cell development and cancer cells, has been recently approved to treat chronic, lymphocytic, and other types of leukemia. This study focused on investigating ibrutinib by its electronic transitions, vibrational frequencies, and electrospray mass spectra. The experimental peaks for electronic spectrum were found at 248.0 and 281.0 nm, whereas the $\nu C=0$ stretching frequency was found at 1652.4 and 1639.19 cm^{-1}. These experimental properties were compared with the corresponding theoretical calculations in which density functional theory was applied. The optimized structure was obtained with the calculations using a hybrid function (B3LYP) and high-level basis sets [6-311G++(d,p)]. Most of the calculated vibrational frequencies showed a relatively good agreement with the experimental ones. The electronic transitions of ibrutinib calculated using time-dependent DFT method were performed at two different solvation methods: PCM and SMD. The mass spectrum of ibrutinib, its fragments, and its isotopic pattern agreed well with the expected spectra.

1. Introduction

The current knowledge in biology and chemistry improved our understanding of cancer treatments. For example, most cancer types express some specific dysregulated molecules called tumor-specific antigens that will play an important role in the tumor development process. Bruton's tyrosine kinase is an enzyme that is important in B-cell development [1–3]. Inhibition of this enzyme is found to cure various types of diseases such as B-cell lineage cancerous, including mainly different types of leukemias common in adults. Although chemotherapy kills the BTK-lineage cells, it also kills other vital cells in the body. However, the recent discovery of molecules specific to BTK enzyme inhibition energizes the kinase-inhibition field research [4–16].

The covalent BTK inhibitors attract great attention because it irreversibly forms a covalent bond with cysteine base (noncatalytic Cys481) located at the edge of the ATP-binding BTK which brings a transient inhibition, higher efficiency, and better specificity and duration of drug action [17]. Several studies had been conducted on finding these irreversible inhibitors, which carry based on the structural bioinformatics approach [5, 6]. It is believed that kinase inhibitors dominate more than 30% of the drug-discovery industry [18, 19].

Ibrutinib (or PCI-32765) is the first BTK covalent irreversible inhibitor approved by several health agencies to treat leukemia types. After extensive laboratory studies and clinical experiments, the approval was decided, providing promising treatment results with $IC_{50} = 0.5$ nM [20–25]. Although some chemical properties of ibrutinib had been reported, most importantly, the crystal structure was solvated in different media [26]. However, many other characteristics are yet to be reported, such as structural, vibrational, and electronic properties.

The purpose of this work is to investigate ibrutinib by its UV-Vis, IR, and ESI-MS characteristics. These experimental properties were compared with the corresponding theoretical calculations using the DFT at the B3LYP level of theory and 6-311G++(d,p) basis sets.

2. Materials and Methods

2.1. Materials and Reagents. Ibrutinib was purchased from BLD Pharmatech Ltd. with >98% purity (via MolPort.com). All other reagents and solvents were of spectroscopic grade and bought from Sigma Aldrich.

2.2. Experimental Methods. Ibrutinib's UV spectrum was measured using Perkin Elmer Lamda 35 UV-Vis spectrophotometer at room temperature. Ibrutinib was dissolved and diluted with methanol to a final concentration of $1x10^{-5}$ M. The absorption spectrum was recorded at the range of 200–800 nm with 0.5 nm slit size. FT-IR spectrum was obtained from compact Alpha FT-IR spectrometer (Bruker, Germany). The device has got multireflection ZnSe as attenuated total reflectance (ATR) and deuterated triglycine sulfate (DTGS) as detector. The accuracy of the instrument reaches as low as 0.01 cm^{-1} for wavenumber and 0.1% for transmittance. Ibrutinib was mixed and ground with KBr to make a homogeneous mixture diffused by compression to get a transparent disk. Ibrutinib's mass spectra were measured using positive polarization electrospray ionization coupled with Q-TOF II Bruker high-resolution mass spectrometry. The mass spectrum of different concentrations of ibrutinib in 95% V/V methanol : formic acid solution (the formic acid solution is 5%FA : 95%H2O) was measured using ESI-MS in the range of 10 nM and 1.0 μM. The electrospray was set at a flow rate of 10 uL/min, the capillary tip is set to be at 6000 V voltage, and the temperature is set at 200 C. The parameters such as collision cell RF (400.0 VPP), the reflector (1700 V), the transfer time (28.0 μs), and prepulse storage time (15.0 μs) were found critical in obtaining the best sensitivity measurements for ibrutinib. The tandem mass spectrum (MS^2) was determined at a collision energy of 25 J.

2.3. Computational Methods. The structural properties of ibrutinib were determined using the density functional theory (DFT) with a hybrid function of B3LYP level of theory and a high level of basis sets with two sets of diffuse and polarization functions [6-311G++(d,p)]. The calculations were carried out using Gaussian 09 software [27] to get the most optimized geometry with the lowest energy. The final optimized structure (Figure 1) is then confirmed to have all real vibrational states at the same theory level (no negative vibrational frequency). The time-dependent DFT (TDDFT) calculations were used to determine ibrutinib's optimized structures of the excited states in methanol utilizing two main solvation packages. Polarizable continuum model (PCM) and solvation model based on density (SMD) are widely used in literature as solvation models and will be our choice of TDDFT calculations of electronic transitions.

3. Results

3.1. Experimental Electronic Spectrum. Figure 2 shows the UV-Vis absorption spectrum of ibrutinib. The absorption mainly occurs between 200 nm and 340 nm. Two main peaks that can be recognized in the spectrum are at 248.0 nm with a molar absorptivity of 22889 L/mol.cm and at 281.0 nm with a molar absorptivity of 16004 L/mol.cm. From the relatively high molar absorptivity, one can conclude that these absorptions are allowed spectroscopically.

3.2. Experimental FT-IR Spectrum. The FT-IR spectrum of ibrutinib is depicted in Figure 3. The spectrum shows several noticeable peaks. N-H peaks appeared at 3470.06 cm^{-1} and 3436.95 cm^{-1}. Aromatic and aliphatic C-H peaks are found between 3063.37 and 2885.62 cm^{-1}. Strong peaks at 1652.40 cm^{-1} and 1639.19 cm^{-1} can be assigned for the C=O stretching frequency. The series of other peaks from 1613.07 to 1520 cm^{-1} can be assigned for C=C and C=N stretching frequencies. Bending frequencies of HCN and HCH in addition to υCH, υCC, υOC, and υNC have their peaks between 1483 and 600 cm^{-1}. The strong and obvious peaks are presented in Table 1 with the help of the assignments from the theoretical calculations.

3.3. ESI-MS Spectrum. The positive mode ESI spectrum of 1 μM ibrutinib in methanol solution is shown in Figure 4(a) with the principle peak at m/z = 441.2032. This peak corresponds to the protonated compound $[\text{ibrutinib} + H]^+$ as expected from the methanol electrospray ionization. The peak accuracy is comparable with the estimated one (441.20390) using the high mass spectrometry. The compound can be detected as low as 10 nM with $[\text{ibrutinib} + H]^+$ is the major peak having S/N ~ 10. Figure 5 shows the tandem mass spectrum of ibrutinib in which two main peaks are found at m/z = 304.1178 and m/z = 138.1123.

3.4. Structural Optimization. The structure of ibrutinib was optimized using a high level of DFT theory with hybrid functional B3LYP and 6-311G++(d,p) as basis sets and is shown in Figure 1. The minimum energy of the optimized molecule was computed as −1446.4520836 HF (−39359.9847812 eV). The molecule's point group was decided as C1 with a dipole moment of 4.237 Debye projected from the carbon in the center of the molecule (C8) in-plane tilted toward the oxygen (O20). The bond lengths, bond angles, and torsion angles of the optimized structure are listed in Table S1 (supplementary materials). N-H bonds were found around 1.01 Å, and the C-bond lengths are between 1.08 Å and 1.10 Å as expected. All carbon angles involve O or N were calculated between 104.7 and 108.6. C8-C9-C14 is measured around 140.4, which is relatively large due to the ring fusing. The torsion angles C8-C9-C14-N13 and C8-C9-C14-N15 torsions are almost linear (177.7° and -3.0°), indicating that the fused moiety is planar that agrees with the aromaticity fact. The difference in the bond length between C4-H35 and C4-H34 (1.10 and 1.09 Å) might be evidence of the intramolecular C2-O1···H35 hydrogen bonding.

3.5. Vibrational Frequencies. The vibrational frequencies were calculated using the DFT method at the same level of

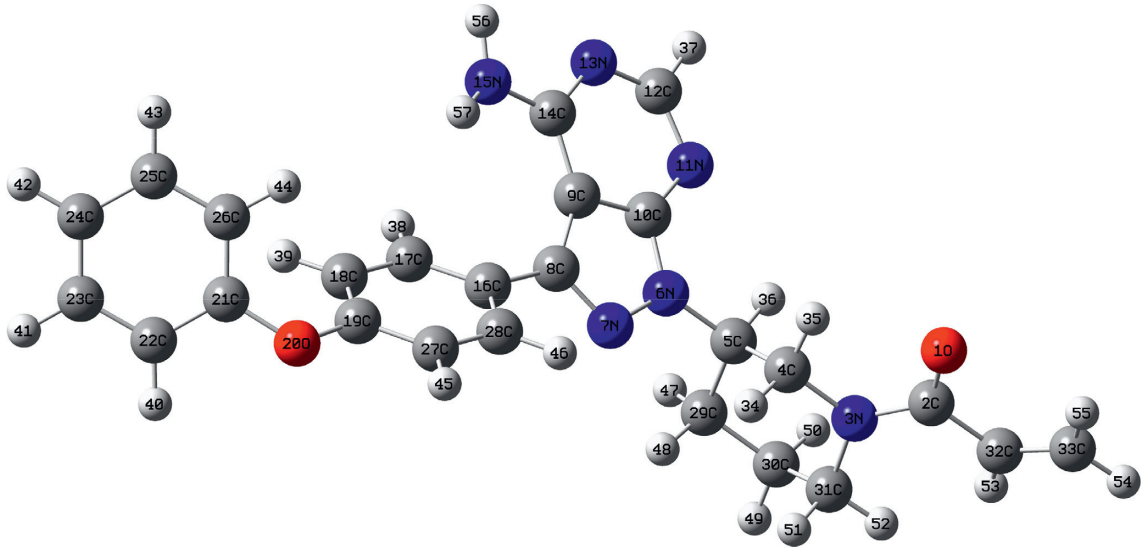

Figure 1: The optimized structure of ibrutinib using high-level density functional theory to identify bond length and bond angles.

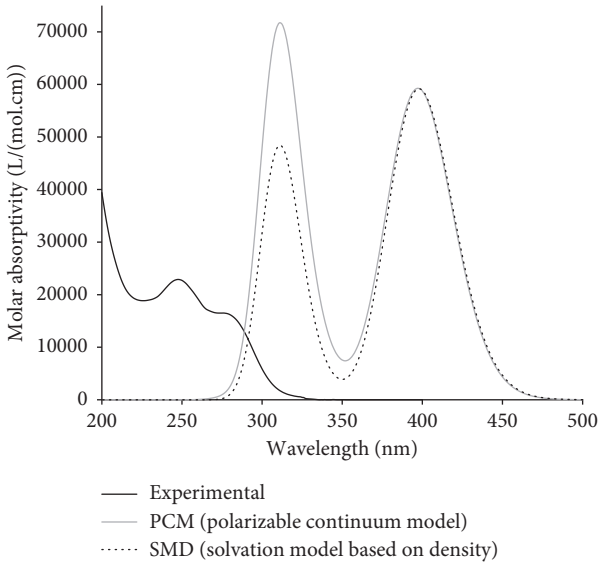

Figure 2: The UV-Vis absorption spectrum of $1x10^{-5}$ M (in methanol) ibrutinib and the density functional theory calculations using two solvation techniques: PCM and SMD. The comparative spectra provide important electronic and orbital information about the molecule.

theory and level of basis sets. The results showed that ibrutinib (57 atoms) has a C1 point group with 165 degrees of freedom that produces 165 IR modes. The main assignments of these IR frequencies are reported in Table 1. The software Veda 4 [28] was used to extract and assign the infrared modes after scaling it with 0.97 as recommended by Andersson and Uvdal [29].

3.6. Electronic Transition. The time-dependent DFT (TDDFT) calculations are determined for all optimized structures. PCM and SMD calculation methods are suggested to estimate the electronic transitions. These calculations computed all molecular orbitals of each molecule, suggesting the possible and most probable electronic transitions. UV-Vis spectrum was constructed based on the energy gaps between states for each structure from these calculations. All calculations were performed using DFT coupled with B3LYP and 6-311G++(d,p) as basis sets. The final results were extracted and visualized using GaussSum [30].

Both PCM and SMD methods predicted almost identical absorption spectra with three peaks. The first peak at 310.13 nm using PCM, 309.28 using the SMD method appeared to be the major one for the PCM method with an oscillator strength of 0.566. The second peak at 399.03 nm (for PCM and 396.26 nm for SMD) is the SMD method's major peak. The last peak is found at 325.98 nm (for PCM and 326.61 nm for SMD) is considered as a minor peak with an oscillator strength of 0.03–0.04. All results are tabulated in Table 2.

4. Discussion

The main functional groups that can be easily distinguished by IR are the N-H and C=O bonds. The υNH_2 stretching frequencies appeared experimentally at 3470.05 and 3436.95 cm^{-1}, while the calculations revealed them at 3600.64 and 3478.42 cm^{-1}. The main reason for a significant shift in the IR in organic compounds is probably due to the hydrogen bonding [31]. In ibrutinib, there might be either intramolecular forces (56H of NH_2 interacting with 13N of pyrimidine) or intermolecular forces of a possible dimerization. This may encounter the difference in the υNH_2 stretching frequency between the theory and the experimental.

Also, υ(O=C) stretching frequencies appeared experimentally at 1652.4 and 1639.19 cm^{-1}, while the DFT estimated them at 1653.85 and 1601.47 cm^{-1}. The two υ(O=C) stretching frequencies differ theoretically at 1.45 and 37.7 cm^{-1} from the experimental. This change is considered

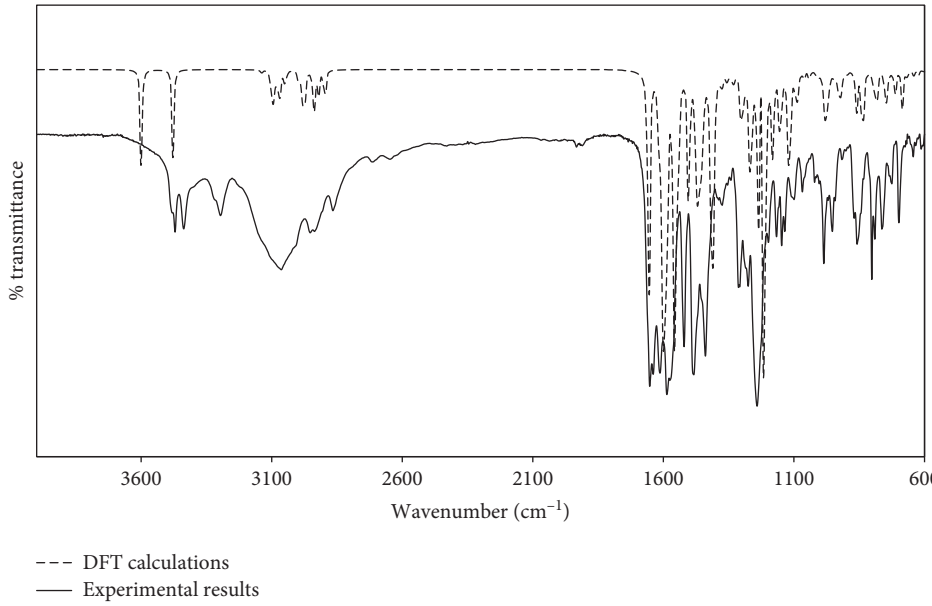

Figure 3: Fourier transform infrared spectrum of ibrutinib. The spectrum is used to determine the molecule's structural information, especially the functional groups N-H_2 (at 3599.6, 3478.0 cm^{-1}) and C=O (at 1652.4, 1639.19 cm^{-1}).

Table 1: The main experimental and calculated vibrational frequencies (in cm^{-1}) and their assignments and contribution for Iibrutinib molecule based on the density functional theory computations at the B3LYP level of theory and 6-311G++(d,p) basis sets.

Experimental frequency (cm^{-1})	Calculated frequency (cm^{-1})	Assignment[a]
3470.05	3600.64	υNH
3436.95	3478.42	υNH
3296.16	3139.9	υCH
3096.16	3094.3	υCH
2952.6	2980.81	υCH
2936.19	2937.16	υCH
2885.62	2893.51	υCH
1652.4	1653.85	υOC
1639.19	1601.47	υOC
1586.75	1557.82	υNC
1520.88	1505.44	υCC
1483.63	1470.52	βHCN
1455.80	1457.4056	βHCH
1312.54	1304.65	υCC
1275.4	1269.73	υNC
1167.02	1182.43	υOC
1147.17	1121.32	υCC
985.52	981.64	υCH
859.31	859.42	υCH, υCC
801.88	833.23	υCH
725.31	745.93	υCH
698.37	684.82	υCC

[a]υ: stretching; β–: bending.

within the agreement between the theory and the experiment encountering the bulkiness of the molecule. Kara et al. concluded that a 20 cm^{-1} difference between B3LYP and experimental for C=O for a relatively medium-sized molecule is a good agreement [32]. Atac et al. suggested that the C=O difference between DFT and experimental can go up to 35 cm^{-1} differences [33]. At the same time, Do et al. found the difference between the theory and the experimental goes up to 58 cm^{-1} for a large molecule like C_{60} fullerenes (even though the molecule is highly symmetric and has no functional group other than C=C) [34].

Other functional groups such as C=C and C=N were laid in 1400–1600 cm^{-1} for both experimental and theoretical calculations. The υCH, υCC, υNC, υOC, βHCH, and βHCN are interfering in the range of 1483–600 cm^{-1}. In general, most of the peaks from the DFT calculations with the high

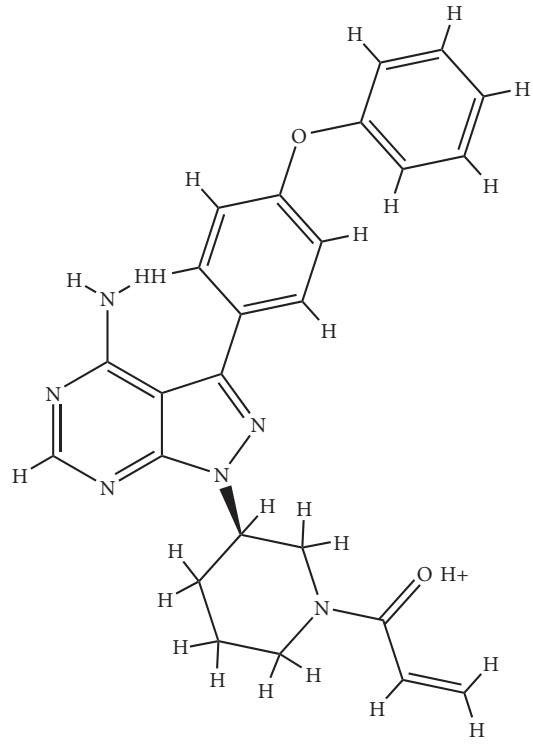

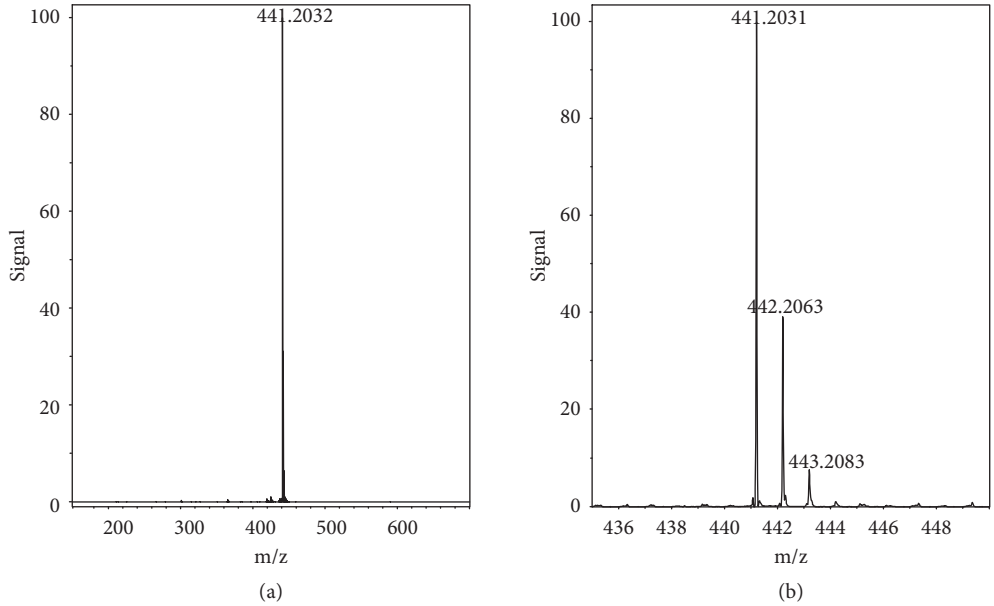

Figure 4: Positive-mode electrospray ionization mass spectrometry of ibrutinib at room temperature with a direct fusion of methanol solution using high-resolution mass spectrometry: (a) full-spectrum and (b) the isotopic pattern.

level of theory and basis sets agreed relatively well with the experimental counterpart peaks, as shown in Table 1 and Figure 3.

On the other hand, the electronic spectrum of ibrutinib showed two peaks at 248.0 and 281.0 nm. In contrast, the calculations revealed two significant peaks at around 310 nm and 399 nm (see Figure 2). These transitions are n-$\pi*$ transitions which are very sensitive to the environment, such as solvent and forces between the functional groups especially with ibrutinib that has many functional groups.

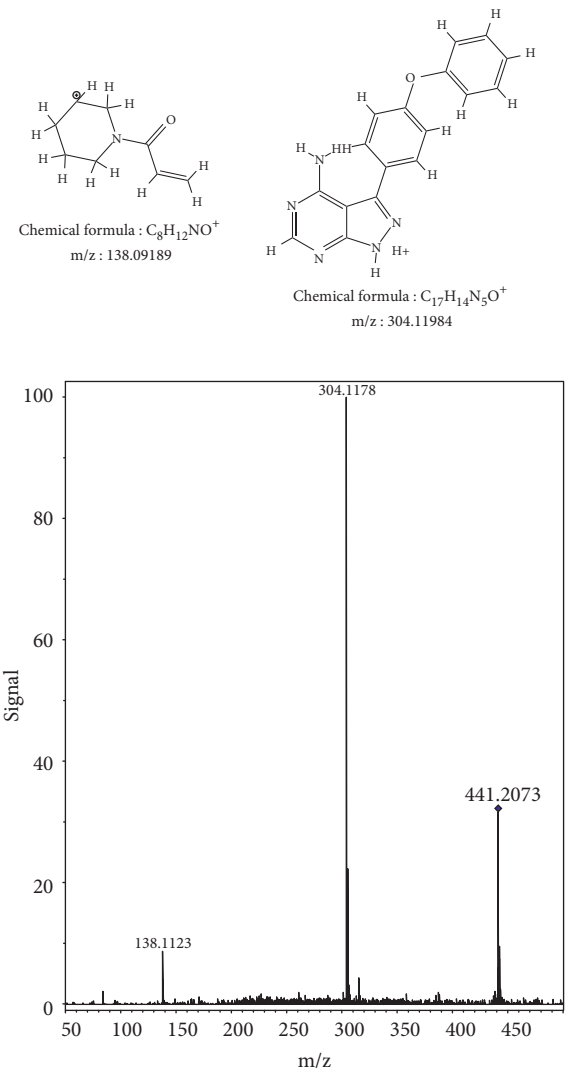

Figure 5: Ibrutinib's tandem mass spectrum with a direct fusion of methanol solution using a high-resolution electrospray ionization mass spectrometer at a collision energy of 25 Joule. Two fragments were found at $m/z = 304.1178$ and 138.1123, corresponding to the pyrazole pyridine bond breakage.

Table 2: The main peaks in the electronic spectrum for ibrutinib calculated by time-dependent density functional theory (B3LYP-6-311G++(d,p)) in methanol using two different solvation methods: polarizable continuum model (PCM) and solvation model based on density (SMD).

Solvation method	Wavelength (nm)	Oscillator strength	Major contribution
PCM	310.13	0.566	HOMO ⟶ LUMO+2 (97%)
SMD	309.28	0.4881	HOMO ⟶ LUMO+2 (96%)
PCM	399.03	0.4641	HOMO ⟶ LUMO (98%)
SMD	396.26	0.5765	
PCM	325.98	0.0416	HOMO⟶ LUMO+1 (99%)
SMD	328.61	0.0338	

The two methods showed little difference from each other in computing the electronic transitions.

The peak at 310.13 (for PCM) nm 309.28 (for SMD) was assigned as HOMO to LUMO +2 electronic transition for both methods. The second peak at 399.03 nm (for PCM and 396.26 nm for SMD) was assigned as HOMO to LUMO with 98% contribution. The last peak found at 325.98 nm (for PCM and 326.61 nm for SMD) is considered a minor peak for the HOMO to LUMO +1 transition (see Table 2). Both methods seem to fail to predict the correct electronic spectra based on the experimental results shown in Figure 2. Although there is a significant difference between the

theoretical and experimental peaks (~61 nm and ~115 nm), in the literature for small organic compounds, the accuracy between the TDDFT methods results in a 15 nm difference (0.3 eV) [35]. On the other hand, the difference in the electronic spectrum, using the best method (B3LYP) for medium-sized molecules (1-naphthol), is estimated as 26 nm (0.29 eV) [36]. One can expect that the existence of many functional groups and the bulkiness of the molecule could result in a greater difference between the theory and experiment, giving the fact that the main transition which is n-$\pi*$ transition is very sensitive to the environment, such as solvent and forces between the functional groups.

The precision of the peak $[\text{ibrutinib} + \text{H}]^+$ in mass spectrometry reached better precision than 2 ppm, which is expected from Bruker QTOF II mass spectrometry. The isotopic pattern of 1 μM ibrutinib is shown in Figure 4(b) with a resolution of 95000 and S/N is larger than 10000. The isotope intensities and values agreed relatively well with the estimated ones obtained from ChemDraw® software. The tandem mass spectrum of ibrutinib (Figure 5) shows two main fragments at $m/z = 304.1178$ and $m/z = 138.1123$ formed from the breaking of the N-C bond between the pyrazole and the piperidine, which agreed with the previous studies of LC-MS of ibrutinib [37–39].

5. Conclusion

This study is the first to investigate the UV-Vis and infrared spectra for ibrutinib. High resolution with isotopic patterned mass spectrum is also reported with a direct infusion of ESI-MS from methanol solution. DFT with a high level of theory, B3LYP, and basis sets, 6-311G++(d,p), is used to determine the optimized geometry of ibrutinib and compare the electronic transitions and vibrational frequencies.

Data Availability

Data are available on request by contacting the author aeyesmaeel@kau.edu.sa or pchem.ismail@gmail.com.

Conflicts of Interest

The author declares no conflicts of interest.

Acknowledgments

This project was funded by the Deanship of Scientific Research (DSR) at King Abdulaziz University, Jeddah, under grant number G-384-662–1439. The author, therefore, acknowledges with thanks DSR for technical and financial support.

Supplementary Materials

Table S1: bond lengths, bond angles, and torsion angles of ibrutinib determined for the optimized molecule by density functional theory study. (*Supplementary Materials*)

References

[1] M. Hojjat-Farsangi, "Targeting non-receptor tyrosine kinases using small molecule inhibitors: an overview of recent advances," *Journal of Drug Targeting*, vol. 24, no. 3, pp. 192–211, 2016.

[2] Y. Nishizuka, "The role of protein kinase C in cell surface signal transduction and tumour promotion," *Nature*, vol. 308, no. 5961, pp. 693–698, 1984.

[3] C. M. Lewis, C. Broussard, M. J. Czar, and P. L. Schwartzberg, "Tec kinases: modulators of lymphocyte signaling and development," *Current Opinion in Immunology*, vol. 13, no. 3, pp. 317–325, 2001.

[4] B. J. Druker, "Molecularly targeted therapy: have the floodgates opened?" *The Oncologist*, vol. 9, no. 4, pp. 357–360, 2004.

[5] Z. Pan, H. Scheerens, S.-J. Li et al., "Discovery of selective irreversible inhibitors for Bruton's tyrosine kinase," *ChemMedChem*, vol. 2, no. 1, pp. 58–61, 2007.

[6] M. S. Cohen, C. Zhang, K. M. Shokat et al., "Structural bioinformatics-based design of selective, irreversible kinase inhibitors," *Science*, vol. 308, no. 5726, pp. 1318–1321, 2005.

[7] D. W. Fry, A. J. Bridges, W. A. Denny et al., "Specific, irreversible inactivation of the epidermal growth factor receptor and erbB2, by a new class of tyrosine kinase inhibitor," *Proceedings of the National Academy of Sciences*, vol. 95, no. 20, pp. 12022–12027, 1998.

[8] Y. Zou, J. Xiao, Z. Tu et al., "Structure-based discovery of novel 4,5,6-trisubstituted pyrimidines as potent covalent Bruton's tyrosine kinase inhibitors," *Bioorganic & Medicinal Chemistry Letters*, vol. 26, no. 13, pp. 3052–3059, 2016.

[9] J. J. M. Rood, S. van Hoppe, A. H. Schinkel, J. H. M. Schellens, J. H. Beijnen, and R. W. Sparidans, "Liquid chromatography-tandem mass spectrometric assay for the simultaneous determination of the irreversible BTK inhibitor ibrutinib and its dihydrodiol-metabolite in plasma and its application in mouse pharmacokinetic studies," *Journal of Pharmaceutical and Biomedical Analysis*, vol. 118, pp. 123–131, 2016.

[10] X. Zhao, M. Xin, Y. Wang et al., "Discovery of thieno[3,2- c] pyridin-4-amines as novel Bruton's tyrosine kinase (BTK) inhibitors," *Bioorganic and Medicinal Chemistry*, vol. 23, no. 17, pp. 6059–6068, 2015.

[11] I. Sagiv-Barfi, H. E. K. Kohrt, D. K. Czerwinski, P. P. Ng, B. Y. Chang, and R. Levy, "Therapeutic antitumor immunity by checkpoint blockade is enhanced by ibrutinib, an inhibitor of both BTK and ITK," *Proceedings of the National Academy of Sciences*, vol. 112, no. 9, pp. E966–E972, 2015.

[12] S. O'Brien, R. R. Furman, S. E. Coutre et al., "Ibrutinib as initial therapy for elderly patients with chronic lymphocytic leukaemia or small lymphocytic lymphoma: an open-label, multicentre, phase 1b/2 trial," *The Lancet Oncology*, vol. 15, no. 1, pp. 48–58, 2014.

[13] M. L. Wang, S. Rule, P. Martin et al., "Targeting BTK with ibrutinib in relapsed or refractory mantle-cell lymphoma," *New England Journal of Medicine*, vol. 369, no. 6, pp. 507–516, 2013.

[14] J. C. Byrd, R. R. Furman, S. E. Coutre et al., "Targeting BTK with ibrutinib in relapsed chronic lymphocytic leukemia," *New England Journal of Medicine*, vol. 369, no. 1, pp. 32–42, 2013.

[15] R. H. Advani, J. J. Buggy, J. P. Sharman et al., "Bruton tyrosine kinase inhibitor ibrutinib (PCI-32765) has significant activity in patients with relapsed/refractory B-cell malignancies," *Journal of Clinical Oncology*, vol. 31, no. 1, pp. 88–94, 2013.

[16] A. Aalipour and R. H. Advani, "Bruton tyrosine kinase inhibitors: a promising novel targeted treatment for B cell lymphomas," *British Journal of Haematology*, vol. 163, no. 4, pp. 436–443, 2013.

[17] J. Singh, R. C. Petter, T. A. Baillie, and A. Whitty, "The resurgence of covalent drugs," *Nature Reviews Drug Discovery*, vol. 10, no. 4, pp. 307–317, 2011.

[18] P. Cohen, "The development and therapeutic potential of protein kinase inhibitors," *Current Opinion in Chemical Biology*, vol. 3, no. 4, pp. 459–465, 1999.

[19] J. J. Wu, M. Z. Zhang, and D. L. Liu, "Acalabrutinib (ACP-196): a selective second-generation BTK inhibitor," *Journal of Hematology and Oncology*, vol. 9, p. 4, 2016.

[20] J. A. Burger, A. Tedeschi, P. M. Barr et al., "Ibrutinib as initial therapy for patients with chronic lymphocytic leukemia," *New England Journal of Medicine*, vol. 373, no. 25, pp. 2425–2437, 2015.

[21] J. R. Brown, J. C. Barrientos, P. M. Barr et al., "The Bruton tyrosine kinase inhibitor ibrutinib with chemoimmunotherapy in patients with chronic lymphocytic leukemia," *Blood*, vol. 125, no. 19, pp. 2915–2922, 2015.

[22] L. A. M. Griner, R. Guha, P. Shinn et al., "High-throughput combinatorial screening identifies drugs that cooperate with ibrutinib to kill activated B-cell-like diffuse large B-cell lymphoma cells," *Proceedings of the National Academy of Sciences of the United States of America*, vol. 111, no. 6, pp. 2349–2354, 2014.

[23] F. Cameron and M. Sanford, "Ibrutinib: first global approval," *Drugs*, vol. 74, no. 2, pp. 263–271, 2014.

[24] J. C. Byrd, J. R. Brown, S. O'Brien et al., "Ibrutinib versus ofatumumab in previously treated chronic lymphoid leukemia," *New England Journal of Medicine*, vol. 371, no. 3, pp. 213–223, 2014.

[25] Administration, U. F. a. D., *IMBRUVICATM (Ibrutinib) Capsules*, FDA, Silver Spring, MA, USA, 2013.

[26] V. Zvoníček, E. Skořepová, M. Dušek et al., "First crystal structures of pharmaceutical ibrutinib: systematic solvate screening and characterization," *Crystal Growth and Design*, vol. 17, no. 6, pp. 3116–3127, 2017.

[27] M. J. Frisch, G. W. Trucks, H. B. Schlegel et al., *Gaussian 09, Revision B.01*, Wallingford, CT, USA, 2009.

[28] M. H. Jamroz, *Vibrational Energy Distribution Analysis VEDA 4*, Warsaw, Poland, 2004-2010.

[29] M. P. Andersson and P. Uvdal, "New scale factors for harmonic vibrational frequencies using the B3LYP density functional method with the triple-ζ basis set 6-311+G (d,p)," *The Journal of Physical Chemistry A*, vol. 109, no. 12, pp. 2937–2941, 2005.

[30] N. M. O'Boyle, A. L. Tenderholt, and K. M. Langner, "cclib: a library for package-independent computational chemistry algorithms," *Journal of Computational Chemistry*, vol. 29, no. 5, pp. 839–845, 2008.

[31] A. J. Barnes, K. Szczpeaniak, and W. J. Orville-Thomas, "Study of intermolecular interactions by matrix isolation vibrational spectroscopy," *Journal of Molecular Structure*, vol. 59, pp. 39–53, 1980.

[32] M. Kara, M. Evecen, and T. Özdogan, "Theoretical investigations on the structural, spectroscopic, electronic and thermodynamic properties of (3-Oxo-3H-benzo[f]chromen-1yl) methyl N,N-dimethylcarbamodithioate-1ex," *Materials Science-Poland*, vol. 35, no. 3, pp. 560–575, 2017.

[33] A. Atac, M. Karabacak, E. Kose, and C. Karaca, "Spectroscopic (NMR, UV, FT-IR and FT-Raman) analysis and theoretical investigation of nicotinamide N-oxide with density functional theory," *Spectrochimica Acta Part A: Molecular and Biomolecular Spectroscopy*, vol. 83, no. 1, pp. 250–258, 2011.

[34] H. Do and N. A. Besley, "Calculation of the vibrational frequencies of carbon clusters and fullerenes with empirical potentials," *Physical Chemistry Chemical Physics*, vol. 17, no. 5, pp. 3898–3908, 2015.

[35] M. Schreiber, M. R. Silva-Junior, S. P. A. Sauer, and W. Thiel, "Benchmarks for electronically excited states: CASPT2, CC2, CCSD, and CC3," *The Journal of Chemical Physics*, vol. 128, no. 13, Article ID 134110, 2008.

[36] J. Wang and B. Durbeej, "How accurate are TD-DFT excited-state geometries compared to DFT ground-state geometries?" *Journal of Computational Chemistry*, vol. 41, no. 18, pp. 1718–1729, 2020.

[37] J. J. M. Rood, P. J. A. Dormans, M. J. van Haren, J. H. M. Schellens, J. H. Beijnen, and R. W. Sparidans, "Bioanalysis of ibrutinib, and its dihydrodiol- and glutathione cycle metabolites by liquid chromatography-tandem mass spectrometry," *Journal of Chromatography B*, vol. 1090, pp. 14–21, 2018.

[38] R. de Vries, M. Huang, N. Bode et al., "Bioanalysis of ibrutinib and its active metabolite in human plasma: selectivity issue, impact assessment and resolution," *Bioanalysis*, vol. 7, no. 20, pp. 2713–2724, 2015.

[39] J. Dong, S. Li, and G. Liu, "In vitro metabolism of ibrutinib in rat, dog and human hepatocytes using liquid chromatography combined with diode-array detection and Q-Exactive Orbitrap tandem mass spectrometry," *Rapid Communications in Mass Spectrometry*, vol. 33, no. 23, pp. 1804–1815, 2019.